Journal of Advanced Ceramics
2018, **7**(2): 99–108
https://doi.org/10.1007/s40145-018-0261-9
ISSN 2226-4108
CN 10-1154/TQ

Research Article

Enhanced time response and temperature sensing behavior of thermistor using Zn-doped $CaTiO_3$ nanoparticles

Subhanarayan SAHOO*

Department of Electrical Engineering, Adani Institute of Infrastructure Engineering, India

Received: November 28, 2017; Revised: January 14, 2018; Accepted: January 23, 2018

Abstract: In the present study, Zn-doped $CaTiO_3$ nanocrystalline was synthesized to study the thermistor behavior with temperature. The X-ray powder diffraction analysis showed the formation of a single-phase orthorhombic structure at room temperature. The electrical resistance of the Zn-doped $CaTiO_3$ increased with increasing doping concentration and decreased at higher measuring temperature, showing a negative temperature coefficient of resistance (NTCR) behavior. Different thermistor parameters were calculated using Steinhart–Hart equations, whilst time domain analysis confirmed faster response towards applied voltage.

Keywords: multiferroic; X-ray diffraction (XRD); electrical properties; conductivity; impedance spectroscopy; NTCR thermistor

1 Introduction

Calcium titanate ($CaTiO_3$) is obtained as an orthorhombic crystal, more specifically the perovskite structure [1]. The Ti centers are octahedral and the Ca centers occupy a cage of 12 oxygen centers. The perovskite structure is versatile and robust, and can be cubic, tetrahedral, or orthorhombic at standard temperatures and pressures. The orthorhombic and tetrahedral geometries differ from the cubic geometry because the dimensions of the unit cells are not equal. Although referred to as the founding father of perovskite, $CaTiO_3$ has not been widely studied, probably because other perovskite, such as $BaTiO_3$ and $SrTiO_3$, are more promising in terms of their technological applications.

Nonetheless, $CaTiO_3$ belongs to an important family of electrical materials, because such materials that have a perovskite structure with a general formula of ABO_3 exhibiting high dielectric constant are of enormous importance to the electronic industry. This is because of their wide applications in capacitor, sensor, actuator, power transmission device, memory device, high-energy storage device, and so forth [2,3].

$CaTiO_3$ is widely applied in specific fields of electronic ceramics including PTC-specific electronic ceramics and ferroelectric ceramic capacitor [4,5]. $CaTiO_3$, an important lead-free perovskite material, has recently attracted great attention from researchers because of its various industrial applications and interesting properties, meaning that recent studies of $CaTiO_3$ have increased. $CaTiO_3$ is paraelectric at room temperature and its dielectric and electrical properties can be modified by various substitutions at the Ca or Ti sites either separately or simultaneously [6]. The applications of modified $CaTiO_3$ are varied and include use in fluorescent lamp, cathode ray tube, plasma display panel ($CaTiO_3:Pr^{3+}$) [7], solid oxide fuel cell ($CaFe_xTi_{1-x}O_3$) [8], solar energy conversion, rechargeable battery, nonlinear optical device (polyaniline–$CaTiO_3$) [9], wireless communication

* Corresponding author.
E-mail: subhanarayan.sahoo@aiim.ac.in

application ($CaTiO_3$–$NdGaO_3$ [10], $CaTiO_3$–$LaGaO_3$ [11], and $CaTiO_3$–$SmGaO_3$ [12]), dielectric barrier in barrier discharge plasma reactor ($Ca_{0.9}Sr_{0.1}TiO_3$) [13], resonator ($Ca_{1-x}M_x(Ti_{1-x}Li_x)O_{3-3x}F_{3x}$) [14], microwave device (($Zn_{0.65}Mg_{0.35}$)TiO_3–$CaTiO_3$) [15], optics ((Ca, Nd)TiO_3) [16], high-energy storage device, memory device ($Ca_{0.5+x}Nd_{0.5-x}(Ti_{0.5}Fe_{0.5})O_3$), fluorescent ((Ca, Zn)$TiO_3$) [17], piezoelectric application (($Na_{0.5}K_{0.5}$)NbO_3–$CaTiO_3$) [18], infrared pyroelectric detector ($Ca_xPb_{1-x}TiO_3$) [19], and so forth. Chemical-based processing routes require several steps, including refluxing, distillation, drying, and high temperature calcination. All these processes require high-purity inorganic or organometallic chemicals as starting materials, which are not only expensive but also highly sensitive to moisture, and therefore require special precaution during handling [20]. These difficulties can be overcome by using mechanical alloying. The general preparation techniques of nanoceramics have been demonstrated widely in the literature [21–28]. The ease with which nanostructured materials can be synthesized is one reason why mechanical alloying has been extensively employed to produce nanocrystalline materials [21].

High-energy ball milling has been used for many years in producing ultra fine powders of nano and submicron sizes. The severe and intense mechanical action on the solid surfaces leads to physical and chemical changes in the near surface region where the solids come into contact under mechanical force. These mechanically initiated chemical and physicochemical effects in solids are generally termed as the mechano-chemical effect. This route is currently being used to synthesize inorganic materials as it exhibits some advantages, such as the reduction in sintering temperature [28,38]. The study of the mechanochemical effect on fine particles has created much interest among researchers because of its several advantages for downstream process like reducing annealing and sintering temperature, reducing phase transformation temperature, enhancing leaching process, decreasing thermal decomposition temperature, and increasing particle reactivity [28,38]. The mechanochemical synthesis process is carried out in high-intensity grinding mills such as vibro mills, planetary mills, and oscillating mills.

The time response is very important for design and analysis of control system. The variation of output with respect to time is known as time response behavior. In time domain system, time is the independent variable. For obtaining satisfactory performance of the system, the behavior of the output with respect to time must be within the specified limit. With the help of time response analysis and corresponding results, the stability, accuracy, and complete evaluation of the system can be easily studied [1–7].

As per literature survey, the picture comes in front that a lot of research is goining on ZnO to establish its potential in electronic industry in terms of different applications. Zn-doped $CaTiO_3$ is reported as bioceramic in medical and fluorescent fields [17]. This leads to do some experiments and to find out its potential in the field of electrical and electronic applications. The present study reports on the enhanced time response behavior of thermistor using Zn-doped $CaTiO_3$ nanoparticles.

2 Experimental procedure

The nanoceramic compounds with the general formula $Ca_{1-x}Zn_xTiO_3$ (x = 0.01, 0.03, 0.05, 0.07) were prepared using corresponding oxides of Ca_2O_3, ZnO, and TiO_2 (purity > 99%; all procured from M/S Loba Chemicals). The nanoparticles of the above materials were prepared using a high-energy ball milling technique. The formation of pure-phase compounds and the basic crystal structure of the samples were checked using the X-ray powder diffraction (XRD) technique. The diffraction data and profile were recorded by a Philips X-ray diffractometer using Cu Kα radiation (wavelength (λ) = 1.5405 Å) in a wide range of Bragg angle 2θ lying between 20° and 80° at a scanning rate of 3 (°)/min at room temperature.

The powders of different samples were cold-pressed separately into small circular pellets with diameter of 1 cm and thickness of 1–2 mm at a pressure of 5×10^6 N/m^2 using a hydraulic press. Polyvinyl alcohol (PVA) was used as the binder to fabricate the pellets. The pellets were sintered at an optimized temperature 1200 ℃ for 4 h.

The parallel surfaces of each circular pellet of the different samples were polished and electroded using air-drying silver paint for the electrical measurements. Electrical parameters including impedance and resistance of the materials were measured as a function of frequency (1 kHz–1 MHz) at different measuring temperatures (300–500 ℃) with an interval of 2.5 ℃ using a phase sensitive LCR/impedance meter (PSM1735, N4L).

3 Results and discussion

Figure 1 shows the XRD analysis of the 15 h milled samples without any external heat treatment at room temperature. The structures remain invariant (orthorhombic) in spite of Zn doping in the x range of 0.01 to 0.07. The XRD patterns confirm the formation of Zn-doped $CaTiO_3$ (ZCT) after 5 h milling and the pure phase is observed above 7 h milling. The peaks are shown to shift to lower angles with increasing Zn content which means peak broadening is occurring as the increasing content of Zn. The lattice parameters were calculated and found to be well matched with the standard values (JCPDS Card No. 42-0423). The XRD of Zn-doped $CaTiO_3$ can be compared to pure un-doped $CaTiO_3$ [38]. Table 1 shows the different values of lattice parameters and crystallite size of ZCT nanoceramics. However, the crystallite sizes remain below 30 nm and the lattice parameters remain unchanged.

The results presented below can be compared to un-doped $CaTiO_3$ nanoceramic [38] which shows similar nature of graph with the variations of data points. $CaTiO_3$ nanoceramic is already proven for a potential candidate as thermistor and temperature sensing component [38]. Due to the same nature of electrical and electronic properties, ZCT also can be reported as a potential candidate as thermistor and temperature sensing component in electronic industry.

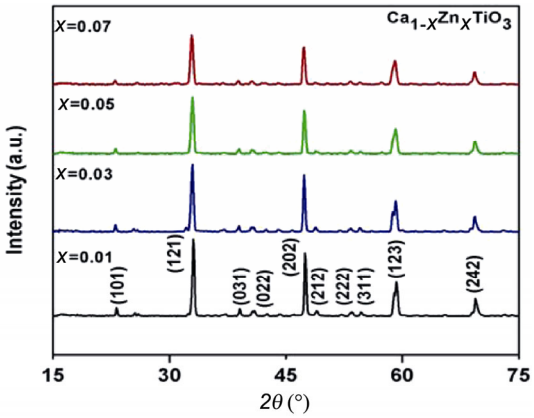

Fig. 1 XRD patterns of $Ca_{1-x}Zn_xTiO_3$ (x = 0.01, 0.03, 0.05, 0.07) at room temperature.

Table 1 Comparison of unit cell parameters and crystallite size of $Ca_{1-x}Zn_xTiO_3$ (x = 0.01, 0.03, 0.05, 0.07)

Composition	Lattice parameter (Å)			Crystallite size (nm)
	a	*b*	*c*	
x = 0.01	5.45	5.40	7.65	25.3
x = 0.03	5.45	5.39	7.63	24.1
x = 0.05	5.41	5.40	7.66	22.3
x = 0.07	5.45	5.40	7.63	25.9

3.1 Electrical resistance of ZCT

We have measured the electrical resistance for calculation of different thermistor parameter in ZCT. Figure 2 shows temperature dependence of electrical resistivity curve for ZCT. By increasing the Zn concentration, the resistance value of the bulk sample gradually increases, showing a clear movement from conductive state to insulating state. At x = 0.01, the resistance value is ~0.9 MΩ at 300 ℃, being 100 times greater than that of the un-doped $CaTiO_3$ sintered at 1200 ℃, which shows that at this condition, the sample property moves from a conductive to an insulating state. However, at x = 0.03, the resistance value increases twice that of the resistance value at x = 0.01, and at x = 0.05 and 0.07, resistance value increases around 2.5 times the resistance of the sample of x = 0.01. Lower electrical variation also occurs between samples of x = 0.05 and x = 0.07 at all temperature range (300–500 ℃). The above discussion suggests that electrical tailoring occurs at all doping concentrations of ZCT.

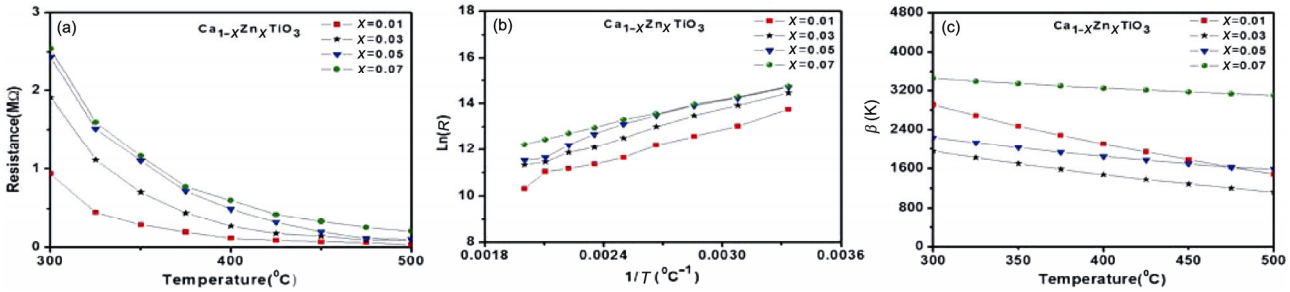

Fig. 2 (a) Temperature dependence of resistance of $Ca_{1-x}Zn_xTiO_3$ (x = 0.01, 0.03, 0.05, 0.07). (b) Natural logarithmic scale of resistance at different Zn concentrations (x = 0.01, 0.03, 0.05, 0.07) with inverse of temperature. (c) Temperature dependence of β at different Zn concentrations (x = 0.01, 0.03, 0.05, 0.07).

It is found that NTCR thermistors follow the Arrhenius equation in the measuring temperature range between 300 and 500 ℃. Figure 2(b) shows that a good linear relationship, indicating excellent NTCR characteristics, is obtained for ZCT [30–32]. As we know, for NTCR thermistors, resistance as a function of temperature can be stated as

$$R_T \propto \exp(1/T) \tag{1}$$

where R_T denotes resistance at respective temperature. By taking natural log of both sides of the equation, the relationship becomes:

$$\ln(R_T) = C + 1/T \tag{2}$$

The above equation satisfies the behavior of a straight line. From this, we can conclude that the graphs shown in Fig. 2(b) are following the above equation as they are showing a straight line behavior [33,34], indicating that all the samples show suitability for use in the thermistor industry as they follow an Arrhenius relationship which is a key factor regarded by many researchers [35]. The variations in graphs of different samples of ZCT due to variations in processing parameter, sintering effect, and doping concentration are similar to the variations found in the analyzed data of Fig. 2(b).

3. 2 Thermistor constant *β* or sensitivity

Figure 2(c) shows the temperature dependence of β value for all compositions of ZCT. It signifies that the prepared ceramic samples are preferred for thermistor due to their gentle slope in β factor. The β values of samples in processing temperature range from 300 to 500 ℃ are shown at different synthesis parameters such as high-energy ball milling effect, sintering effect, and doping concentration variation [23]. The temperature dependent β value is indicated in Fig. 2(c). The β value is also used to calculate the temperature coefficient of resistance or the α value.

The equation for thermistor constant β using Steinhart–Hart coefficient [4] is

$$\beta = \sqrt{\left(\frac{b}{3c}\right)^3 + \frac{\alpha^2}{4}} \tag{3}$$

The sensitivity of a thermistor for temperature sensing is described by its activation energy. All four samples from this study exhibit different slopes and activation energies, which are shown in Table 2.

The values of activation energy were calculated by the following formula [33,36–38]:

$$E_a = k_B \times \beta \tag{4}$$

where E_a is the activation energy, k_B is the Boltzmann constant, and β is the thermistor constant.

These observed values for the activation energy of the prepared ceramic samples may be due to the presence of charge carriers inside the grain and some extrinsic charge carriers created owing to the use of silver electrodes at elevated temperatures. The activation energy and thermistor constant show transition from higher to lower values, with both these factors being important from the point of view of applications. For NTCR thermistor materials, the β constant is closely related to resistance [39] as shown in Fig. 3, so the search for different pairs requires complete formulation changes. β is the material constant, which indicates the relationship between material resistance and temperature [37,40]:

$$R = A\exp\left(\frac{\beta}{T}\right) \tag{5}$$

Table 2 Sensitivity of $Ca_{1-x}Zn_xTiO_3$ (x = 0.01, 0.03, 0.05, 0.07)

Measuring temperature (℃)	Sintering temperature 1200 ℃							
	$Ca_{0.09}Zn_{0.01}TiO_3$		$Ca_{0.07}Zn_{0.03}TiO_3$		$Ca_{0.05}Zn_{0.05}TiO_3$		$Ca_{0.03}Zn_{0.07}TiO_3$	
	β (K)	E_a (eV)	β (K)	E_a (eV)	β (K)	E_a (eV)	β (K)	E_a (eV)
300	2909	0.25	1955	0.17	2242	0.19	3448	0.30
325	2685	0.23	1822	0.16	2131	0.18	3393	0.29
350	2478	0.21	1699	0.15	2030	0.17	3342	0.29
375	2286	0.19	1585	0.14	1936	0.17	3295	0.28
400	2106	0.18	1480	0.13	1849	0.16	3251	0.28
425	1938	0.16	1383	0.12	1769	0.15	3210	0.28
450	1780	0.15	1292	0.11	1694	0.15	3173	0.27
475	1630	0.14	1208	0.1	1624	0.14	3137	0.27
500	1488	0.12	1129	0.09	1588	0.14	3104	0.27

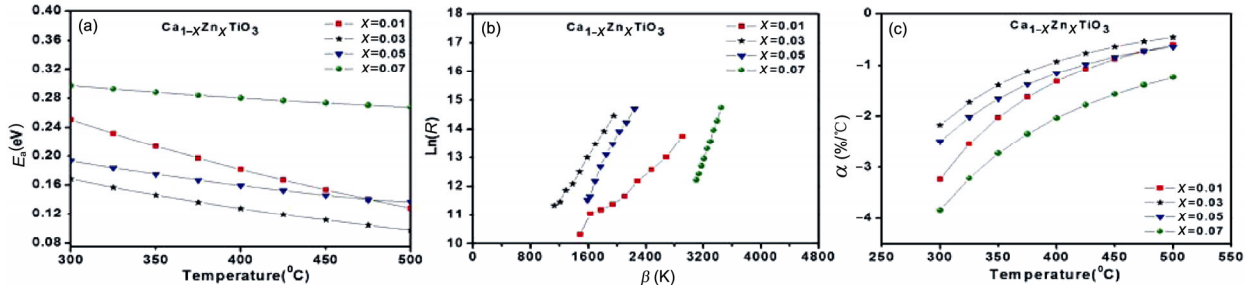

Fig. 3 (a) Temperature dependence of activation energy calculated at different Zn concentrations (x = 0.01, 0.03, 0.05, 0.07). (b) Natural logarithmic scale of resistance with β value at different Zn concentrations (x = 0.01, 0.03, 0.05, 0.07). (c) Temperature dependence of α at different Zn concentrations (x = 0.01, 0.03, 0.05, 0.07).

where R is the electrical resistance, T is the temperature (℃), and β is the exponential factor.

By taking the natural log of the above equation, the relationship becomes:

$$\ln(R) = C + \frac{\beta}{T} \tag{6}$$

where C is a constant factor.

The above equation shows the linear relationship between β and the natural logarithm of resistance, which we can see in Fig. 3(b) [41].

Temperature dependent activation energy graphs can be seen in Fig. 3(a), with these following a similar trend to those seen in the temperature dependent sensitivity plots of Fig. 2(c). This signifies the relationship between the activation energy and β value, which is mathematically proven by Eq. (6) [23]. All the graphs demonstrate the prepared samples' potential towards NTCR behavior in the specified temperature range. Also, the linearity behavior with respect to temperature makes the prepared samples very suitable for any thermistor-based device applications. The linear relationship that can be seen in Fig. 3(b) shows that the prepared samples follow an Arrhenius relationship between β and logarithmic resistance values [29]. All of the graphs fit with the straight line equation, thus showing linearity behavior that is an important factor of any material performance at the device level. Based on the above analyses, all the prepared samples prove their potential to be used as thermistor in any electrical device. β decreases with temperature, as shown in Fig. 2(c), meaning that activation energy variation with respect to temperature in the specified temperature range is obtained from this study.

3. 3 Sensitivity of ZCT

Table 2 shows the tailoring of the sensitivity index and activation energy (E_a) in the specified temperature range (300–500 ℃) with the concentration of ZCT, showing a lower sensitivity index than the un-doped $CaTiO_3$ [38]. As the concentration of Zn increases from x = 0.01 to 0.03, the sensitivity of the material decreases; however, suddenly at x = 0.05 it starts increasing in between the values of x = 0.01 and 0.03. Upon further increasing to x = 0.07, the sensitivity index also continues to increase greater than that of x = 0.01. The sensitivity index at x = 0.07 reaches the highest value of all samples sintered at the same temperature (1200 ℃). The sensitivities of different materials reported by other authors are presented in Table 3.

3. 4 Temperature coefficient of resistance

The temperature coefficient of resistance or α was determined from resistance–temperature characteristic measurements. The temperature coefficient is commonly expressed in percentage per degree centigrade (%/℃) [30,34–36]. For NTCR thermistor, the resistance exponential function of temperature has similarity with α value, and is nonlinear across the measuring temperature range [5,32,33]. The equation for α value using Steinhart–Hart coefficient [24,27,37,38] is stated as follows:

$$\alpha = \frac{a - 1/T}{c} = -\frac{\beta}{T^2} \times 100 \tag{7}$$

α decreases with an increase in β constant [39], which can be seen if the graphs from Figs. 2(c) and 3(c) are compared.

3. 5 Stability factor

We conducted simple stability tests [27] using the stability factor formula [14,24], which is related as the ratio of maximum resistance to minimum resistance.

Table 3 Sensitivity of different materials

No.	Material	Sensitivity β (K)	Reference
1	Ag_2S–Ag	1250–2684	[41]
2	$Ni_{0.6}Mn_{2.4-x}Sn_xO_4$	3993–4639	[42]
3	$Mn_{1.5-x}Co_{1.5}Ni_xO_4$	4427–2134	[43]
4	La–Mn–Al–O	1065–537	[44]
5	$CaCu_{3-x}Mn_xTi_4O_{12}$ ($0 \leqslant x \leqslant 1$)	5488–8031	[45]
6	$Mn_{1.56}Co_{0.96}Ni_{0.48}O_4$	2972–3035	[46]
7	$Mn_{1.05-y}Co_{1.95-x-z-w}Ni_xMg_yAl_zFe_wO_4$	3318–3771	[47]
8	Mn–Co–Ni	3500	[48]
9	$BaFe_xNb_xTi_{1-2x}O_3$	1284–3574	[49]
10	$Cu_{0.2}Ni_{0.5}Zn_{1.0}Mn_{1.3}O_4$, $Cu_{0.25}Ni_{0.5}Zn_{1.0}Mn_{1.25}O_4$, and $Cu_{0.4}Ni_{0.5}Mn_{2.1}O_4$	2632–3424	[50]
11	Mn–V–O	1393–5208	[51]
12	La_2O_3-doped $0.6Y_2O_3$–$0.4YCr_{0.5}Mn_{0.5}O_3$	3600–11936	[52]
13	$Cu_{0.2}Ni_{0.5}Zn_{1.0}Mn_{1.3}O_4$	3356	[53]
14	Mixture of spinel material and RuO_2	4045	[54]
15	Ni–Mn–Co–O	3478–3847	[55]
16	$Ni_{0.6}Cu_{0.4}Mn_2O_4$	1937–3208	[56]
17	$LaNiO_3 + NiMn_2O_4$	5000	[57]
18	$BaCo^{II}_xCo^{III}_{2x}Bi_{1-3x}O_3$	1140–1234	[58]
19	Fe^{3+}-doped $Ni_{0.9}Co_{0.8}Mn_{1.3-x}Fe_xO_4$ ($0.6 \leqslant x \leqslant 0.7$)	3103–3355	[59]
20	$Ni_{0.6}Mg_{0.3}Mn_{1.5-x}Al_{0.6+x}O_4$ (x = 0, 0.1, 0.2, 0.4, 0.6)	4165–5301	[60]
21	$Ni_{0.6}Si_{0.2}Al_{0.6}Mn_{1.6}O_4$	4817–5166	[61]
22	$NiMg_xMn_{2-x}O_4$	3825–4144	[62]
23	Sr–Bi–Mn–Fe–O	3141–3693	[63]
24	$NiMnCo_xFe_{1-x}O_4$ (x = 0.25, 0.5, 0.7, 0.8, 0.9)	1396–7245	[64]
25	$BaBi_{1-x}Sb_xO_3$ ($0 \leqslant x \leqslant 0.5$)	3392–5762	[65]
26	$BaY_xBi_{1-x}O_3$	2890–3392	[66]
27	$YCr_{1-x}Mn_xO_3$	3896–11520	[67]
28	$Ni_{1-x}Cu_xMn_2O_4$ ($0 \leqslant x \leqslant 1$)	1164–1397	[68]
29	$Mn_{0.43}Ni_{0.9}CuFe_{0.67}O_4$	1500–2000	[69]
30	$SrFe_{0.9}Sn_{0.1}O_{3-\delta}$	2611–3558	[70]

From the tests, we observe the broadening and narrowing of data points in a specified or fixed temperature limit. For $CaTiO_3$ nanocrystaline, the data point narrowing occurs by reduction of 50% compared to the sample prepared by the conventional method, whereas the sintering temperature decreases as the data point broadening doubles (Table 4). As Zn concentration increases, data point narrowing occurs. The above analysis shows that ZCT is a potential candidate for thermistor having good performance and good stability factor as shown in Table 4.

Table 4 Stability factor of $Ca_{1-x}Zn_xTiO_3$ (x = 0.01, 0.03, 0.05, 0.07)

Doping concentration	R_{max}/R_{min}	Stability factor $\log(R_{max}/R_{min})$
x = 0.01	30.8	1.49
x = 0.03	22.7	1.36
x = 0.05	23.9	1.37
x = 0.07	12.5	1.09

3.6 Time domain analysis

The present study focused on the time response analysis of ZCT for NTCR thermistor sensing behavior. Input signal was analyzed by using equivalent circuit Cole–Cole plots (fitted by Z-View) and from the equivalent circuit transfer function of different samples at 300 ℃. After obtaining the transfer function, input temperature signal was performed as step signal by using partial fraction and inverse Laplace transformation, and the time dependent equation was obtained. By using time dependent equation, the response graph was plotted and time domain specifications were observed with the help of MATLAB simulation as shown in Fig. 4.

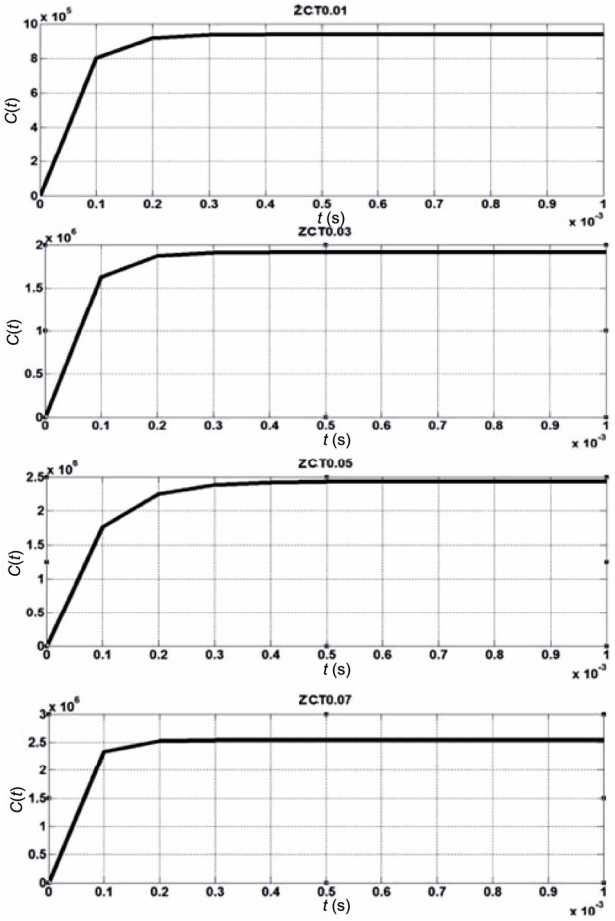

Fig. 4 Time response analysis of $Ca_{1-x}Zn_xTiO_3$ (x = 0.01, 0.03, 0.05, 0.07).

3. 7 Time response

The time response is very important for design and analysis of control system. The variation of output with respect to time is known as time response behavior. In time domain system, time is the independent variable. For obtaining satisfactory performance of the system, the behavior of the output with respect to time must be within the specified limits. With the help of time response analysis and corresponding results, the stability, accuracy, and complete evaluation of the system can be easily studied [1–7].

There are two parts of the time response of any system: transient response and steady state response. The time from the initiation of the input signal to the settling time of a control system is the transient period and beyond the settling time steady state appears. It can be stated in three different ways as (1) delay time, which is the time required to reach 50% of the final value, for the very first time; (2) settling time, which is defined as the time taken by the response to reach and stay at a constant value; and (3) time constant, which is the time required for the output to rise 63.2% of final or steady state value.

We consider the disc pellets as a system, where temperature acts as an input step signal, and output signal is observed in the form of electrical parameters such as resistance and capacitance. The delay time, settling time, and time constant are calculated for each particular temperature for a comparison point of view.

3. 8 Time response analysis of ZCT

From the curve fitting of the polar plot by Z-View, we discover that the equivalent circuit of the curves of all samples prepared from nano-ZCT is R C .The equations of the time domain response are derived below .

3. 9 For $Ca_{0.99}Zn_{0.01}TiO_3$

The transfer function of the disc thermistor prepared from $Ca_{0.99}Zn_{0.01}TiO_3$ nanomaterial sintered at 1200 ℃ is given as follows:

$$\frac{C(s)}{R(s)} = \frac{R}{1+RCs}$$

$$\Rightarrow \frac{C(s)}{R(s)} = \frac{938780}{1+938780\times 5.5497E-11\times s}$$

$$\Rightarrow C(s) = 938780\left(\frac{1}{s} - \frac{1}{s+19194.05187}\right)$$

Taking inverse Laplace transform on both sides, the time dependent equivalent equation of $Ca_{0.99}Zn_{0.01}TiO_3$ sintered at 1200 ℃ is

$$C(t) = 938780\left(1-\mathrm{e}^{-19194.05187t}\right) \quad (8)$$

Similar calculations are performed for other compositions to obtain the time response factor.

For $Ca_{0.97}Zn_{0.03}TiO_3$, $Ca_{0.95}Zn_{0.05}TiO_3$, and $Ca_{0.93}Zn_{0.07}TiO_3$, the equations are found to be respectively:

$$C(t) = 1912500\left(1-\mathrm{e}^{-19032.35238t}\right)$$

$$C(t) = 2433500\left(1-\mathrm{e}^{-12854.84275t}\right)$$

$$C(t) = 2539400\left(1-\mathrm{e}^{-25177.02254t}\right)$$

Time domain specifications of $Ca_{1-x}Zn_xTiO_3$ are given in Table 5. We obtained interesting results by doping Zn in $CaTiO_3$, with all Zn-doped samples showing much faster response rates than un-doped $CaTiO_3$ sintered at the same temperature (1200 ℃), i.e., approximately 10 times faster response in the case of doped samples than that of the un-doped $CaTiO_3$ [38]. As Zn concentration increases, the system moves faster, which can be used in the industry as a good temperature sensor. All the time domain response graphs evolved by deriving the above equations are shown in Fig. 4.

4 Conclusions

Zn-doped $CaTiO_3$ nanocrystalline was prepared by high-energy ball milling. The as prepared powders possessed single-phase orthorhombic structure at room temperature. Transmission electron microscope study confirmed that particle size is below 50 nm. We have carried out electrical resistance measurements and calculated different thermistor parameters which showed that Zn-doped $CaTiO_3$ can be used as a potential candidate in thermistor application at high temperatures. Time domain analysis showed that by doping Zn, the

Table 5 Time domain specification of $Ca_{1-x}Zn_xTiO_3$ (x = 0.01, 0.03, 0.05, 0.07)

Composition	Code	Sintering temperature (℃)	Delay time t_d (ms)	Settling time t_s (ms)	Time constant (ms)
$Ca_{0.99}Zn_{0.01}TiO_3$	ZCT0.01	1200	0.06	0.40	0.07
$Ca_{0.97}Zn_{0.03}TiO_3$	ZCT0.03	1200	0.06	0.35	0.075
$Ca_{0.95}Zn_{0.05}TiO_3$	ZCT0.05	1200	0.07	0.55	0.08
$Ca_{0.93}Zn_{0.07}TiO_3$	ZCT0.07	1200	0.05	0.28	0.08

samples became more reliable towards temperature sensing with faster response.

References

[1] Buttner RH, Maslen EN. Electron difference density and structural parameters in $CaTiO_3$. *Acta Cryst* 1992, **B48**: 644–649.

[2] Wang H, Cheng J, Zhai L, *et al*. Preparation of $Li_xCa_{1-x}TiO_3$ solid electrolytes by the sol–gel method. *Solid State Commun* 2007, **142**: 710–712 .

[3] Murashkina AA, Demina AN, Filonova EA, *et al*. Thermal expansion and electrical conductivity of $CaTi_{0.9}M_{0.1}O_{3-\delta}$ (M = Fe, Cu, Al). *Inorg Mater* 2008, **44**: 296–298.

[4] Dunyushkina LA, Demin AK, Zhuravlev BV. Electrical conductivity of iron-doped calcium titanate. *Solid State Ionics* 1999, **116**: 85–88.

[5] Chen L, Fan H, Zhang M, *et al*. Phase structure, microstructure and piezoelectric properties of perovskite $(K_{0.5}Na_{0.5})_{0.95}Li_{0.05}NbO_3$–$Bi_{0.5}(K_{0.15}Na_{0.85})_{0.5}TiO_3$ lead-free ceramics. *J Alloys Compd* 2010, **492**: 313–319.

[6] Gheorghies C, Boutinaud P, Loic M, *et al*. Results on nanosized $CaTiO_3$:Pr^{3+} phosphor. *J Optoelectron Adv M* 2009, **11**: 583–589.

[7] Ahmed MA, Bishay ST. Effect of annealing time, weight pressure and Fe doping on the electrical and magnetic behavior of calcium titanate. *Mater Chem Phys* 2009, **114**: 446–450.

[8] Parinitha M, Venkateshulu A. Synthesis, characterization and transport property of PANI–calcium titanate composites. *International Journal of Latest Research in Science and Technology* 2013, **2**: 495–498.

[9] Suvorov D, Valant M, Jančar B, *et al*. $CaTiO_3$-based ceramics: Microstructural development and dielectric properties. *Acta Chem Slov* 2001, **48**: 87–99.

[10] Li R, Yamaguchi Y, Tang Q, *et al*. Liquid phase sintering of $Ca_{0.9}Sr_{0.1}TiO_3$ dielectric ceramics. *J Ceram Soc Jpn* 2004, **112**: S309–S312.

[11] Murugan M, Kakate VK, Bapat MS. Synthesis, characterization and evaluation of reflectivity of nanosized $CaTiO_3$/epoxy resin composites in microwave bands. *Bull Mater Sci* 2011, **34**: 699–704.

[12] Taibi-Benziada L, Mezroua A, von der Mühll. $CaTiO_3$ related materials for resonators. *Ceram-Silikaty* 2004, **48**: 180–184.

[13] Yuan Y, Zhang S, Zhou X, *et al*. Low-temperature sintering and microwave dielectric properties of $(Zn_{0.65}Mg_{0.35})TiO_3$–$CaTiO_3$ ceramics with H_3BO_3 addition. *Ceram-Silikaty* 2009, **53**: 5–8.

[14] Marques VS, Cavalcante LS, Sczancoski JC, *et al*. Synthesis of (Ca,Nd)TiO_3 powders by complex polymerization, Rietveld refinement and optical properties. *Spectrochim Acta A* 2009, **74**: 1050–1059.

[15] Shah MR, Akther Hossain AKM. Structural, dielectric and complex impedance spectroscopy studies of lead free $Ca_{0.5+x}Nd_{0.5-x}(Ti_{0.5}Fe_{0.5})O_3$. *J Mater Sci Technol* 2013, **29**: 323–329.

[16] Yuan X, Shi X, Shen M, *et al*. Luminescent properties of Pr^{3+} doped (Ca, Zn)TiO_3: Powders and films. *J Alloys Compd* 2009, **485**: 831–836.

[17] Chang R-C, Chu S-Y, Lin Y-F, *et al*. The effects of sintering temperature on the properties of $(Na_{0.5}K_{0.5})NbO_3$–$CaTiO_3$ based lead-free ceramics. *Sensor Actuat A: Phys* 2007, **138**: 355–360.

[18] Chewasatn S, Milne SJ, Pankurddee N, *et al*. Sol–gel synthesis of crack-free thin films of calcium lead titanate. In Proceedings of the 10th IEEE International Symposium on Applications of Ferroelectrics, 1996, **2**: 597–600.

[19] Parashar SKS, Choudhary RNP, Murty BS. Ferroelectric phase transition in $Pb_{0.92}Gd_{0.08}(Zr_{0.53}Ti_{0.47})_{0.98}O_3$ nanoceramic synthesized by high-energy ball milling. *J Appl Phys* 2003, **94**: 6091–6096.

[20] Suryanarayana C. Mechanical alloying and milling. *Prog Mater Sci* 2001, **46**: 1–184.

[21] Abreu Jr. A, Zanetti SM, Oliveira MAS, *et al*. Effect of urea on lead zirconate titanate–Pb$(Zr_{0.52}Ti_{0.48})O_3$–nanopowders synthesized by the Pechini method. *J Eur Ceram Soc* 2005, **25**: 743–748.

[22] Koch CC, Suryanarayana C. Nanocrystalline materials. In *Microstructure and Properties of Materials*. Li JCM, Ed. Singapore: World Scientific Publishing Corp., 2000, **2**: 359–403.

[23] Suryanarayana C. Mechanical alloying. In *ASM Handbook, Vol. 7, Powder Metal Technologies and Applications*. ASM International, Materials Park, **1998**: 80–90.

[24] Suryanarayana C, Koch CC. Nanostructured materials. In *Non-Equilibrium Processing of Materials*. Suryanarayana C, Ed. Oxford, UK: Elsevier Science Pub., **1999**: 313–346.

[25] Ma E, Atzmon M. Phase transformations induced by mechanical alloying in binary systems. *Mater Chem Phys* 1995, **39**: 249–267.

[26] Morrell S, Man YT. Using modelling and simulation for the design of full scale ball mill circuits. *Miner Eng* 1997, **10**: 1311–1327.

[27] Misra A, Cheung J. Particle motion and energy distribution in tumbling ball mills. *Powder Technol* 1999, **105**: 222–227.

[28] Sahoo S, Dash U, Parashar SKS, *et al*. Frequency and temperature dependent electrical characteristics of $CaTiO_3$ nano-ceramic prepared by high-energy ball milling. *J Adv Ceram* 2013, **2**: 291–300.

[29] Brunets I, Mrooz O, Shpotyuk O, *et al*. Thick-film NTC thermistors based on spinel-type semiconducting electroceramics. In Proceedings of the 24th International Conference on Microelectronics, 2004, **2**: 503–506.

[30] Gouda GM, Nagendra CL. A new transition metal oxide sensor material for thermistor applications: Manganese–vanadium–oxide. In Proceedings of the 1st International Symposium on Physics and Technology of Sensors, 2012:

125–128.

[31] McMurtry CH, Terrell WT, Benecki WT. A tin oxide thermistor for temperature sensing to 1800 °F. *IEEE Trans Ind Gen A* 1966, **2**: 461–464.

[32] Yuan CL, Liu XY, Xu JW, *et al*. Electrical properties of $Sr_xBa_{1-x}Fe_{0.6}Sn_{0.4}O_{3-\delta}$ NTC thermistor. *Bull Mater Sci* 2012, **35**: 425–431.

[33] Park K, Bang DY, Kim JG, *et al*. Influence of the composition and the sintering temperature on the electrical resistivities of Ni–Mn–Co–(Fe) oxide NTC thermistors. *Journal of the Korean Physical Society* 2002, **41**: 251–256.

[34] De Vasconcelos EA, Khan SA, Zhang WY, *et al*. Highly sensitive thermistors based on high-purity polycrystalline cubic silicon carbide. *Sensor Actuat A: Phys* 2000, **83**: 167–171.

[35] Yuan C, Liu X, Liang M, *et al*. Electrical properties of Sr–Bi–Mn–Fe–O thick-film NTC thermistors prepared by screen printing. *Sensor Actuat A: Phys* 2011, **167**: 291–296.

[36] Nenova ZP, Nenova TG. Linearization circuit of the thermistor connection. *IEEE T Instrum Meas* 2009, **58**: 441–449.

[37] Jadhav RN, Mathad SN, Puri V, *et al*. Studies on the properties of $Ni_{0.6}Cu_{0.4}Mn_2O_4$ NTC ceramic due to Fe doping. *Ceram Int* 2012, **38**: 5181–5188.

[38] Sahoo S, Parashar SKS, Ali SM. $CaTiO_3$ nano ceramic for NTCR thermistor based sensor application. *J Adv Ceram* 2014, **3**: 117–124.

[39] Gouda GM, Nagendra CL. Structural and electrical properties of mixed oxides of manganese and vanadium: A new semiconductor oxide thermistor material. *Sensor Actuat A: Phys* 2009, **155**: 263–271.

[40] Roy TK, Sanyal D, Bhowmick D, *et al*. Temperature dependent resistivity study on zinc oxide and the role of defects. *Mat Sci Semicon Proc* 2013, **16**: 332–336.

[41] Sagar R, Madolappa S, Sharanappa N, *et al*. Synthesis, structure and electrical studies of praseodymium doped barium zirconium titanate. *Mater Chem Phys* 2013, **140**: 119–125.

[42] Tsao K-Y, Tsai C-S, Huang C-Y. Effect of argon plasma treatment on the PTC and NTC behaviors of HDPE/carbon black/aluminum hydroxide nanocomposites for over-voltage resistance positive temperature coefficient (PTC). *Surf Coat Technol* 2010, **205**: S279–S285.

[43] Zhang H, Chang A, Guan F, *et al*. The optimal synthesis condition by sol–gel method and electrical properties of $Mn_{1.5-x}Co_{1.5}Ni_xO_4$ ceramics. *Ceram Int* 2014, **40**: 7865–7872.

[44] Xiong X, Xu J, Zhao P, *et al*. Structural and electrical properties of thick film thermistors based on perovskite La–Mn–Al–O. *Ceram Int* 2014, **40**: 10505–10510.

[45] Zhang B, Zhao Q, Chang A, *et al*. New negative temperature coefficient thermistor ceramics in Mn-doped $CaCu_{3-x}Mn_xTi_4O_{12}$ ($0 \leqslant x \leqslant 1$) system. *Ceram Int* 2014, **40**: 11221–11227.

[46] Gao YQ, Huang ZM, Hou Y, *et al*. Structural and electrical properties of $Mn_{1.56}Co_{0.96}Ni_{0.48}O_4$ NTC thermistor films. *Mat Sci Eng B* 2014, **185**: 74–78.

[47] Xia J, Zhao Q, Gao B, *et al*. Preparation and electrical properties of $Mn_{1.05-y}Co_{1.95-x-z-w}Ni_xMg_yAl_zFe_wO_4$ NTC ceramic derived from microemulsion method. *J Alloys Compd* 2014, **591**: 207–212.

[48] Kong W, Chen L, Gao B, *et al*. Fabrication and properties of $Mn_{1.56}Co_{0.96}Ni_{0.48}O_4$ free-standing ultrathin chips. *Ceram Int* 2014, **40**: 8405–8409.

[49] Luo Y, Li X, Liu X, *et al*. Study of microstructure and electrical properties of $BaNb_xFe_xTi_{1-2x}O_3$ ($0 < x \leqslant 0.1$) negative temperature coefficient materials. *Mater Lett* 2013, **93**: 187–189.

[50] Aleksic OS, Nikolic MV, Lukovic MD, *et al*. Preparation and characterization of Cu and Zn modified nickel manganite NTC powders and thick film thermistors. *Mat Sci Eng B* 2013, **178**: 202–210.

[51] Gouda GM, Nagendra CL. Preparation and characterization of thin film thermistors of metal oxides of manganese and vanadium (Mn–V–O). *Sensor Actuat A: Phys* 2013, **190**: 181–190.

[52] Zhang B, Zhao Q, Chang A, *et al*. La_2O_3-doped $0.6Y_2O_3$–$0.4YCr_{0.5}Mn_{0.5}O_3$ composite NTC ceramics for wide range of temperature sensing. *J Alloys Compd* 2013, **581**: 573–578.

[53] Aleksic OS, Nikolic MV, Lukovic MD, *et al*. Analysis and optimization of a thermal sensor system for measuring water flow. *Sensor Actuat A: Phys* 2013, **201**: 371–376.

[54] Jagtap S, Rane S, Gosavi S, *et al*. Infrared properties of '*lead free*' thick film NTC thermo-resistive sensor based on the mixture of spinel material and RuO_2. *Sensor Actuat A: Phys* 2013, **197**: 166–170.

[55] Muralidharan MN, Rohini PR, Sunny EK, *et al*. Effect of Cu and Fe addition on electrical properties of Ni–Mn–Co–O NTC thermistor compositions. *Ceram Int* 2012, **38**: 6481–6486.

[56] Jadhav RN, Mathad SN, Puri V. Studies on the properties of $Ni_{0.6}Cu_{0.4}Mn_2O_4$ NTC ceramic due to Fe doping. *Ceram Int* 2012, **38**: 5181–5188.

[57] Kang J-E, Ryu J, Han G, *et al*. $LaNiO_3$ conducting particle dispersed $NiMn_2O_4$ nanocomposite NTC thermistor thick films by aerosol deposition. *J Alloys Compd* 2012, **534**: 70–73.

[58] Yuan CL, Liu XY, Zhou CR, *et al*. Electrical properties of lead-free thick film NTC thermistors based on perovskite-type $BaCo^{II}_xCo^{III}_{2x}Bi_{1-3x}O_3$. *Mater Lett* 2011, **65**: 836–839.

[59] Wang J, Zhang J. Structural and electrical properties of $NiMg_xMn_{2-x}O_4$ NTC thermistors prepared by using sol–gel derived powders. *Mat Sci Eng B* 2011, **176**: 616–619.

[60] Liang S, Zhang X, Bai Y, *et al*. Study on the preparation and electrical properties of NTC thick film thermistor deposited by supersonic atmospheric plasma spraying. *Appl Surf Sci* 2011, **257**: 9825–9829.

[61] Liang S, Yang J, Yi X, *et al*. An efficient way to improve the electrical stability of $Ni_{0.6}Si_{0.2}Al_{0.6}Mn_{1.6}O_4$ NTC thermistor. *Ceram Int* 2011, **37**: 2537–2541.

[62] Wang J, Zhang J. Structural and electrical properties of $NiMg_xMn_{2-x}O_4$ NTC thermistors prepared by using sol–gel derived powders. *Mat Sci Eng B* 2011, **176**: 616–619.

[63] Yuan C, Liu X, Liang M, *et al*. Electrical properties of Sr–Bi–Mn–Fe–O thick-film NTC thermistors prepared by screen printing. *Sensor Actuat A: Phys* 2011, **167**: 291–296.

[64] Zhao J, Li L, Gui Z. Influence of lithium modification on the properties of Y-doped $Sr_{0.5}Pb_{0.5}TiO_3$ thermistors. *Sensor Actuat A: Phys* 2001, **95**: 46–50.

[65] Jadhav RN, Mathad SN, Puri V. Studies on the properties of $Ni_{0.6}Cu_{0.4}Mn_2O_4$ NTC ceramic due to Fe doping. *Ceram Int* 2012, **38**: 5181–5188.

[66] Luo Y, Li X, Liu X. Electrical properties of binder-free thick film $BaY_xBi_{1-x}O_3$ NTC thermistors. *J Alloys Compd* 2011, **509**: 463–465.

[67] Kamlo AN, Bernard J, Lelievre C, *et al*. Synthesis and NTC properties of $YCr_{1-x}Mn_xO_3$ ceramics sintered under nitrogen atmosphere. *J Eur Ceram Soc* 2011, **31**: 1457–1463.

[68] Singla ML, Sharma S, Raj B, *et al*. Characterization of transition metal oxide ceramic material for continuous thermocouple and its use as NTC fire wire sensor. *Sensor Actuat A: Phys* 2005, **120**: 337–342.

[69] Jin X, Chang A, Zhang H, *et al*. A comparison study of sinterability and electrical properties for microwave and conventional sintered $Mn_{0.43}Ni_{0.9}CuFe_{0.67}O_4$ ceramics. *J Mater Sci Technol* 2010, **26**: 344–350.

[70] Yuan C, Wu X, Huang J, *et al*. Electrical properties of thick film NTC thermistors based on $SrFe_{0.9}Sn_{0.1}O_{3-\delta}$. *Solid State Sci* 2010, **12**: 2113–2119.